



# Quantifying the effect of grain size on weathering of basaltic powders: Implications for negative emission technologies via soil carbon sequestration



Elizabeth Vanderkloot <sup>\*</sup>, Peter Ryan

Department of Earth and Climate Sciences, Middlebury College, Middlebury, VT, 05753, USA

## ARTICLE INFO

Editorial Handling by: Thomas Gimmi

**Keywords:**

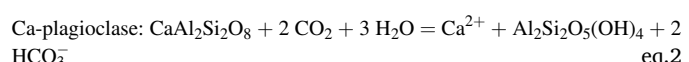
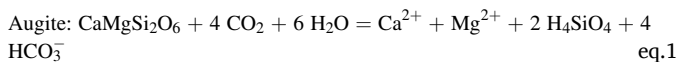
Enhanced rock weathering  
ERW  
Carbon sequestration  
Net emission technology  
Basalt  
Tropics

## ABSTRACT

Weathering of basaltic powders was studied experimentally at 35 °C in dilute solutions of oxalic acid and carbonic acid to assess the effect of grain size and reactive surface area for materials under consideration for carbon dioxide reduction (CDR) by enhanced rock weathering (ERW). The basalts chosen for this study (with their mineralogical compositions) are the Blue Ridge (BR) meta-basalt (chlorite > epidote > plagioclase > actinolite) and Pioneer Valley (PV) basalt (plagioclase > augite > quartz > chlorite). Powders of BR and PV basalts were sieved into <45 μm, 45–150 μm, and >150 μm fractions, and experiments were performed in open-system reactors designed to simulate a 1 mm thick layer of basalt added to agricultural soil in the humid tropics. Weathering rate was assessed by measuring the flux of base cations leached from silicate minerals and results indicate that silt-dominated basaltic powder (<45 μm) weathers at approximately double the rate of sand dominated (150–500 μm) basaltic powder, both for the BR and PV basalts. This study estimates CDR rates between 2.8 and 6.8 t CO<sub>2</sub>/ha/yr across the range of grain size fractions analyzed. Etched primary mineral grains (e.g. plagioclase, augite, actinolite) with depleted base cations observed by SEM-EDS provide morphological and stoichiometric evidence of dissolution, as do the presence of frayed chlorite grains that contain adsorbed Ca and are compositionally intermediate to end-member chlorite and smectite. Small amounts of micron-scale calcite were also observed as a precipitate on mineral surfaces, likely a consequence of localized saturation of Ca and HCO<sub>3</sub> in the matrix of the weathering powders. The results of this study help to constrain differences in weathering flux as a function of grain size, with important implications for effectiveness of CDR via ERW.

## 1. Introduction

The weathering of silicate minerals is a known sink for CO<sub>2</sub>, and growing concern about global climate change and the need for a portfolio of strategies has spurred interest in applying powdered basaltic rocks to agricultural lands in order to enhance carbon dioxide reduction (CDR) from atmosphere to soils (Beerling et al., 2020; Lewis et al., 2021). Basalt is a common widespread rock type. Weathering reactions of two common igneous minerals (augite, Ca-plagioclase) show reaction stoichiometries and the way in which carbon dioxide is converted to dissolved bicarbonate by chemical weathering of silicates:



The bicarbonate on the products side becomes available for storage in soils or transport via soil drainage to groundwater and streams for eventual long-term storage in the oceans (Beerling et al., 2020). The weathering of augite as shown here is an example of congruent weathering whereas weathering of plagioclase shown here is incongruent and results in dissolved Ca and bicarbonate as well as the mineral kaolinite.

Information from laboratory and field experiments (Kelland, 2020; Amann et al., 2020, and Dietzen et al., 2018) and modeling (Beerling et al., 2020; Lewis et al., 2021; Rinder and von Hagke, 2021) has been applied to quantifying CDR by what is commonly termed enhanced rock weathering (ERW) or enhanced mineral weathering (EMW), and estimates range from rates as low as 0.1 tonnes CO<sub>2</sub>/ha/year to as high as 12 tonnes CO<sub>2</sub>/ha/year (ten Berge et al., 2012; Renforth et al., 2015;

\* Corresponding author.

E-mail address: [evanderkloot@middlebury.edu](mailto:evanderkloot@middlebury.edu) (E. Vanderkloot).

Dietzen et al., 2018; Amann et al., 2020; Kelland, 2020; Lewis et al., 2021). The variability in estimates calls for more experimental determinations of weathering rates (Calabrese et al., 2022), especially given the many factors that will influence CDR by ERW, including (1) differences in mineral weathering rates among the main basaltic minerals (Lewis et al., 2021), (2) regional climate, where rates are greater in environments featuring high temperature and precipitation (White et al., 1999; Pincus et al., 2017), (3) the role of microbial populations (Banfield and Nealson, 1997), and (4) differences in grain size, geometry and reactive surface area (Holdren and Speyer, 1987; Anbeek, 1993; Brantley, 2008; Bray et al., 2015; Rinder and von Hagke, 2021). CDR by ERW is predicted to be most effective where rock powders contain minerals that weather rapidly, in moist and warm environments, with microbial populations that accelerate rate, and where powders are fine-grained. The latter variable – differences in grain size and reactive surface area – is the main focus of this study, which seeks to quantify the effect of grain size on weathering of basaltic powders in an experimental setting designed to represent weathering in the humid tropics.

This study reports on experimental weathering of basaltic powders as a function of grain size comparing two basaltic rocks commonly used in CDR. In this case, weathering is quantified by measuring the flux of base cations leached from basaltic powder over the course of the experiment. The experimental parameters were designed to simulate tropical field conditions, where a dilute oxalic + carbonic acid solution was added to basaltic powders and allowed to react at 35 °C. Leached solutions that percolated through the powdered basalt were collected for chemical analysis; weathering flux is determined by measurements of dissolved cations leached into experimental soil solutions as dictated by the stoichiometry of weathering reactions. Weathered residual solids were analyzed by SEM-EDS to assess textural evidence of weathering (e.g. pitting) as well as potential formation of secondary solid phases (Yokoyama and Banfield, 2002).

We hypothesize that weathering flux will increase with decreasing grain size, and that the experimental approach employed in this study will provide useful information on weathering potential as a function of grain size for two common basalts in consideration for CDR by means of ERW.

## 2. Materials and methods

### 2.1. Basaltic powders

Information pertaining to mineralogy and chemical composition are presented in Tables 1 and 3–5. Grain size of Blue Ridge Basalt (“BR”, supplied by Rock Dust Local, Bridport, Vermont USA) was already known to be sufficiently fine grained (Lewis et al., 2021) so as to not require further mechanical grain size reduction. Pioneer Valley Basalt (“PV”) powder (also supplied by Rock Dust Local) was further crushed to reduce grain size in a Shatterbox 8515 rock crusher then separated into coarse, medium and fine size fractions using sieves of 500 μm, 150 μm, and 45 μm openings, resulting in three dry-sieved size fractions labeled as follows:

Blue Ridge Basalt: BR-coarse (500–150 μm), BR-medium (150–45 μm), and BR-fine (<45 μm).

Pioneer Valley Basalt: PV-coarse (500–150 μm), PV-medium (150–45 μm), and PV-fine (<45 μm).

**Table 1**

Information about the two basaltic powders examined in this study.

Sample ID	Description
Blue Ridge Metabasalt (“BR”)	Greenstone from Blue Ridge Province, Virginia USA, likely Proterozoic Catoctin Formation.
Pioneer Valley Basalt (“PV”)	Unmetamorphosed basaltic rock from the Holyoke Range, Central Massachusetts USA, likely Jurassic in age Blue Ridge Metabasalt and Pioneer Valley Basalt are supplied by Rock Dust Local LLC, Bridport Vermont USA

**Table 2**

Results of grain size separation by sieving of Blue Ridge Basalt (BR) and Pioneer Valley Basalt (PV), as determined by laser diffraction grain size analysis.

Sample	Mean (μm)	Medium (μm)	Mode (μm)
BR Coarse	502.4	479.2	484.1
BR Medium	32.2	14.8	10.8
BR Fine	9.96	8.68	9.44
<hr/>			
PV Coarse	265.4	259.3	366.3
PV Medium	60	52.7	72.3
PV Fine	10.3	7.49	8.23

The three subsamples each of BR and PV were then analyzed as separate samples provided by the methods below.

### 2.2. Weathering reactor set-up

A weathering experiment was conducted using laboratory-scale weathering reactors (Fig. 1) to simulate the weathering of basalts in a tropical environment. In total, seven weathering reactors were constructed, including one for each grain size (fine, medium, and coarse) for each sample and one blank (to assess background concentrations of the solutions used in the weathering experiment). Each of the seven reactors contained 100 g of an unreactive substrate (Ultra-Pure PTFE boiling stones) which were placed on top of three Whatman #40 filter paper in a cylindrical container of 10 cm diameter with a perforated bottom. On top of the boiling stone layer were three additional Whatman #40 filter papers. Atop that, 15 g of powdered basalt fractions were spread evenly on top of the filter paper in 6 (3 × 2) reactors. In the case of the blank, no powdered basalt was added atop the PTFE boiling stones and filters. Each container sat on top of an 800 mL beaker 10 cm in diameter sealed with parafilm and covered with a watch glass to prevent evaporation from the beaker and/or cylindrical container. The recoveries of the solution at the bottom of the beaker indicated no measurable evaporation. The reactors were placed into a 35 °C oven during the duration of the experiment to simulate soil surface temperature on a typical hot day in the tropics (Lal, 1995). The oven temperature did not change to simulate temperature differences during the evening and night. The 35 °C soil temperature was maintained throughout the entire experiment.

The liquid (“soil solution”) in this experiment was a solution of 15 mmol 1<sup>-1</sup> oxalic acid in carbonated milliQ water at an initial pH of 1.6. The carbonated water solution is assumed to be saturated with respect to CO<sub>2</sub> and was achieved by pumping carbon dioxide into MilliQ deionized water in an acid-washed 1 L bottle using a SodaStream countertop device. Addition of oxalic acid at low concentration is designed to simulate the chelating effect of organic acids present in natural solutions (Rozalén et al., 2014), and after the first rinse (washing of exchangeable cations, with pH ~ 2), all solutions collected had pH values between 3.4 and 4.2, moderately acidic yet comparable to the acidic end-member of Oxisol soil solutions (Pincus et al., 2017).

100 mL of milli Q with 15 mmol 1<sup>-1</sup> oxalic acid was added to reaction chambers six times over the course of two weeks. This was done to simulate the amount of precipitation tropical croplands might receive in said period (to simulate mean annual precipitation of 2500 mm/yr, typical of a tropical monsoon climate; Rohli and Vega, 2015), which amounts to 13 mm of rain every two days. Leachate pooled at the bottom of each reactor and was collected in containers 48–72 h after each incidence of “watering.” The leachate from each reactor for each round was later decanted, filtered, preserved with dilute HNO<sub>3</sub> (also to mimic matrix of ICP-MS standards) and saved for ICP-MS analysis. On the final day, leachate was collected, and then 100 mL of Milli-Q water was added to flush out the reactor and collect the remaining liquid that was still held in the soil; this approximated 100 mL. This last leachate was again decanted after the soils had the liquid flushed out. It is important to note that the experimental approach employed herein did not allow for analysis of concentrations of solids that remained in the basalt-PTFE

**Table 3**

Mineral abundances (wt %) determined by XRD and XRF in the two powdered basalts as a function of sieved grain size fractions. Note specifically the differences in composition between the BR fractions e.g. increasing chlorite abundance with decreasing grain size.

Weight Percent of Minerals Present in Samples							
	Plagioclase	Fe-Ti Oxides	Quartz	Amphibole	Epidote	Chlorite	Other
<b>BR-coarse</b>	23	2	6	14	35	19	1
<b>BR-medium</b>	20	1	5	12	26	36	0
<b>BR-fine</b>	16	1	4	9	19	51	0
	Plagioclase	Pyroxene	Fe-Ti Oxides	Quartz		Other	
<b>PV-coarse</b>	50	42	5		1		2
<b>PV-medium</b>	44	49	5		1		1
<b>PV-fine</b>	35	55	6		1		3

**Table 4**

Chemical compositions of BR and PV powdered rock size fractions. The data are for anhydrous (post-LOI) fused glass discs. Raw data including analyses of certified standards (SRM 688, BCR-2) are presented in [Table S1](#).

	<u>SiO<sub>2</sub></u>	<u>TiO<sub>2</sub></u>	<u>Al<sub>2</sub>O<sub>3</sub></u>	<u>Fe<sub>2</sub>O<sub>3</sub></u>	<u>MnO</u>	<u>MgO</u>	<u>CaO</u>	<u>Na<sub>2</sub>O</u>	<u>K<sub>2</sub>O</u>	<u>P<sub>2</sub>O<sub>5</sub></u>	<u>SUM</u>	<u>Sr</u>	<u>Zr</u>
	%	%	%	%	%	%	%	%	%	%	%	ppm	ppm
BR fine	45.25	1.55	15.04	15.19	0.26	11.97	7.23	2.83	0.55	0.15	100	90.0	109.9
BR medium	45.62	1.96	15.14	14.30	0.22	9.14	10.59	2.40	0.42	0.16	100	170.2	103.2
BR coarse	46.63	1.95	16.11	13.63	0.20	7.14	11.29	2.53	0.36	0.16	100	229.2	108.5
PV fine	49.59	0.94	11.95	17.59	0.27	5.98	10.57	2.41	0.69	<0.10	100	179.2	139.4
PV medium	51.19	0.82	12.59	15.05	0.23	6.16	10.02	3.21	0.65	0.10	100	138.3	103.1
PV coarse	52.41	0.88	13.75	13.96	0.21	5.44	9.39	3.04	0.81	0.10	100	156.6	101.5

“soil”, so in this respect, results are constrained to measuring weathering flux by leaching of base cations.

### 2.3. XRD

Basaltic powders were randomly oriented into topload sample holders and scanned at Middlebury College using a D8ADVANCE Bruker X-ray diffractometer using CuK $\alpha$  radiation, a solid-state Si (Li) detector, over an angular range of 3–40° 2 $\theta$  continuously scanned at 2.5 min per degree. Mineral identification was done using Bruker EVA software with reference data from the International Center for Diffraction Data (ICDD, formerly JCPDS). Mineral abundances were assessed by measuring peak areas and then comparing peak intensities of mineral peaks to in-house reference intensities; these estimates were then refined using chemical data from XRF, effectively by performing normative calculations using mineral chemistry data from SEM-EDS and the literature.

### 2.4. SEM/EDS pre- and post- weathering

Scanning electron microscopy (SEM) was used to analyze morphology, relative grain sizes of each sample, and chemical compositions. Powders were carbon-coated and examined using a Tescan Vega 3 LMU SEM at Middlebury College with Energy Dispersive X-ray Spectroscopy (EDS) and Electron Backscatter Diffraction (EBSD) attachments. Operating parameters for imaging included secondary electron imaging (SE), an accelerating voltage of 5 kV, beam intensity of 7.0, and a working distance of 15 mm. Images were taken at various magnifications. EDS analysis includes the insertion of backscatter detectors and an EBSD with operating parameters of 20 kV, a beam intensity of 17.00, and a working distance of 15 mm. Cobalt served as our standard for EDS analysis. Compositions of minerals determined by EDS are presented as molar values based on silicate mineral stoichiometries. Mineral standards used for quantification include the Oxford Instruments Aztec factory standardization library. In addition to SEM-EDS analysis of fresh powders, weathered rock powders for each sample were collected after the leaching experiment was completed. The weathered samples went through the same steps for SEM/EDS analysis.

### 2.5. XRF

XRF analysis was performed for all samples and one standard of two different weights. For each sample, XRF disks were prepared by first measuring out 0.8000 ( $\pm 0.0005$ ) grams of post-LOI powder material into a crucible using a Sartorius CPA225D Competence Analytical Balance. 8.0000 ( $\pm 0.0005$ ) grams of Claisse lithium tetraborate flux was then added to the crucible to create a final flux to sample ratio of 10:1. Due to limited quantities of PV Fine, we measured 0.2724 g of the powder – this encompassed the remaining powder for this size fraction. After, we measured 5.8116 g of Claisse lithium tetraborate flux. This ratio is 20:1. To account for analytical errors, we prepared two XRF disks; one of the standard weight and a second one following the weights measured for the PV Fine fraction. The contents of the crucible were stirred with a glass rod and fused at 1065 °C using the MIDD-XRF Disk method on a LE Neo Fluxer Claisse fusion instrument. All fused disks were labeled and evaluated using a Thermo Fisher Scientific ARL QUANTX EDXRF analyzer at Middlebury College. Accuracy and precision were assessed by running certified basalt standards (SRM-688 and BCR-2) which demonstrate analytical uncertainty for the elements relevant to this study ([Supplemental Table S1](#)). Detection limits ([Table S1](#)) have been determined for this method-instrument combination on-site by analysis of blanks, certified standards, and replicates of samples containing elements at or near the detection limit, and values reported here are well above method detection limits (MDLs). Precision and accuracy of XRF analyses were quantified by replicate analyses of unknowns as well as certified standards. Over the range of concentrations for the elements focused on in this study, precision is as follows: SiO<sub>2</sub> ( $\pm 1.0\%$ , e.g., 58.0  $\pm$  0.58%); Al<sub>2</sub>O<sub>3</sub> ( $\pm 3.0\%$ , e.g. 15.0  $\pm$  0.45%); Fe<sub>2</sub>O<sub>3</sub> ( $\pm 3.0\%$ , e.g. 10.0  $\pm$  0.30%); MgO and CaO ( $\pm 3.0\%$ , e.g. 8.0  $\pm$  0.24%); Na<sub>2</sub>O ( $\pm 5.0\%$ , e.g. 3.0  $\pm$  0.15%). Precision of K<sub>2</sub>O analyses at low concentrations encountered in these mafic powders is poor (e.g.  $\pm 20\%$ ) and K quantification is not featured in data analysis presented herein.

### 2.6. Inductively coupled plasma - mass spectrometry (ICP-MS)

In order to quantify mineral alteration by leaching of cations, solutions derived from leached powders were filtered using 0.45  $\mu$ m syringe

**Table 5**  
Primary mineral composition (from SEM-EDS analysis) and mineral abundances (by XRD and XRF) of powdered basaltic rocks by size fraction.

Sample ID	Primary Minerals			Primary Minerals			Primary Minerals
	Plagioclase	Pyroxene	Fe-Ti Oxides	SiO <sub>2</sub>	Amphibole	Epidote	Chlorite
Blue Ridge (BR)	Na <sub>0.8</sub> Ca <sub>0.2</sub> Al <sub>1.2</sub> Si <sub>2.8</sub> O <sub>8</sub>	—	—	Na <sub>0.2</sub> Ca <sub>1.0</sub> Mg <sub>4.0</sub> Fe <sub>1.7</sub> Al <sub>2.0</sub> Si <sub>6.6</sub> O <sub>22</sub> (OH) <sub>2</sub>	Ca <sub>2</sub> Fe <sub>2</sub> AlSi <sub>3</sub> O <sub>13</sub> H	Mg <sub>3.2</sub> Fe <sub>1.2</sub> Al <sub>1.4</sub> Si <sub>2.9</sub> Al <sub>1.1</sub> O <sub>10</sub> (OH) <sub>8</sub>	
BR-coarse	23	—	2	6	14	35	19
BR-medium	20	—	1	5	12	26	36
BR-fine	16	—	1	4	9	19	51
Pioneer (PV)	Na <sub>0.6</sub> Ca <sub>0.4</sub> Al <sub>1.5</sub> Si <sub>2.5</sub> O <sub>8</sub>	Ca <sub>0.7</sub> Mg <sub>0.7</sub> Fe <sub>0.6</sub> Si <sub>1.9</sub> Al <sub>0.1</sub> O <sub>6</sub>	—	SiO <sub>2</sub>	—	—	—
PV-coarse	50	42	5	1	—	—	—
PV-medium	44	49	5	1	—	—	—
PV-fine	35	55	6	1	—	—	—

**Table 6**

Percentages of each cation lost due to weathering (leached into solution) relative to the original amount in the corresponding rock powder fractions (Table 4), over the course of 14-day experimental weathering. For example, in the case of Mg, 1.82% of Mg was leached out of BR-fine during experimental weathering.

	Si	Al	Fe	Mn	Mg	Ca	Na	K
BR-fine	0.55	1.59	1.21	2.37	1.82	0.36	0.93	3.07
BR-medium	0.53	1.96	0.91	2.86	1.70	0.18	0.84	2.97
BR-coarse	0.28	0.70	0.44	1.37	1.20	0.12	0.48	1.32
PV-fine	0.32	1.58	2.01	2.52	3.26	0.47	1.88	2.18
PV-medium	0.34	1.72	1.41	2.06	2.09	0.38	0.95	1.58
PV-coarse	0.30	1.38	1.87	2.29	2.27	0.24	0.85	0.98

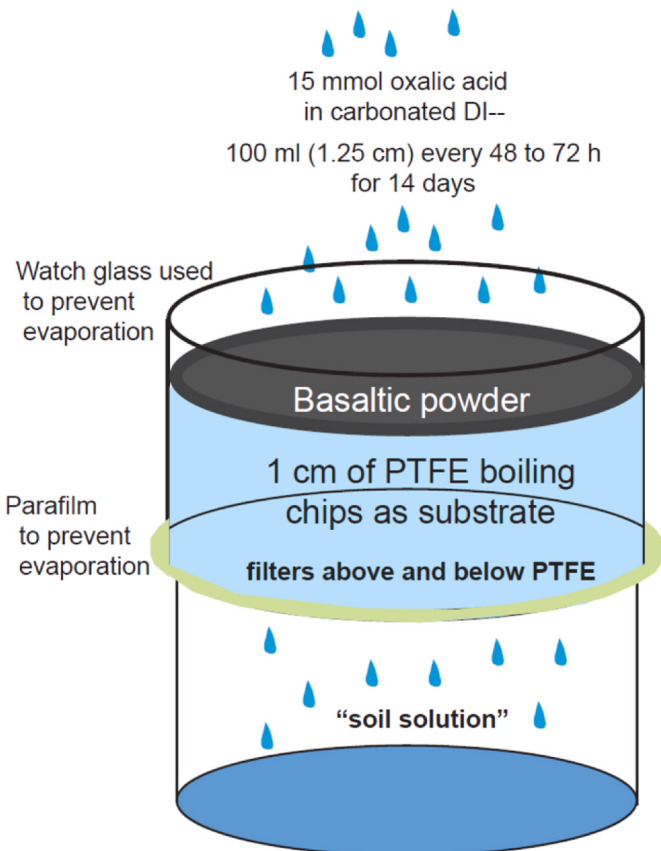


**Fig. 1.** Schematic representation of the experimental weathering chamber, showing a 0.6 mm layer (= 15 g) of basaltic powder applied atop 1 cm of PTFE boiling chips that functioned as a permeable substrate beneath the basalt, with Whatman #40 filters above and below PTFE. Diameter is 10 cm. 100 mL of a dilute solution of oxalic acid in carbonated water was rained on the soils six times over a two-week period, and filtered leachate was collected for ICP-MS analysis to quantify the extent of chemical weathering.

filters and these solutions were analyzed at Middlebury College using a Thermo Fisher iCAPQ ICP-MS in KED mode. Results were converted to mmol/kg to determine liberation by weathering of Ca, K, Na, Mg, and Fe. NIST standard 1643f as well as in-house standards were analyzed in-line and used to correct for drift provided that reported values are within 80–125% of the certified value. Raw ICP-MS data and QC data as well as drift-corrected and molar values are presented in [Supplemental Table S2](#). Analysis of NIST 1643f and in-house standards indicates analytical uncertainty  $\leq 5\%$  of reported values for Mg, Ca, Na, K, Fe and Mn. Analytical uncertainties for Al and Si are  $\sim \pm 10\%$  of reported values. Note that only Mg and Ca are used for CDR calculations.

## 2.7. Laser diffraction grain size analysis

Fresh/unaltered basaltic powders used in the weathering experiments (section 2.6) were mixed with sodium hexametaphosphate (20 mL, 3%) and the samples were capped and mixed. After overnight exposure with the dispersant, the grain size distribution of each sample was measured through laser scattering in a Horiba LA-950 at Middlebury College equipped with an autosampler. This instrument has an effective range from 50 nm to 3 mm, and a refractive index of 1.54 and an imaginary component of 0.1i were employed in calculating the grain size distribution. All samples except PV-fine were rerun as duplicates, and the analyzer was checked before and after each run with in-house standards. Accuracy of the instrument is regularly checked against a NIST 1.0  $\mu\text{m}$  standard (ILot 33084), 500  $\mu\text{m}$  glass beads (Coulter 7800372), and in-house reference materials.

## 3. Results

### 3.1. Laser diffraction grain size analysis

Grain size analysis yields insight into the results of sieving, which in turn allows for assessment of weathering flux as a function of grain size (Fig. 2). The grain size distribution for PV displays three prominent modes in correspondence with our three size fractions: <45  $\mu\text{m}$ , 45–150  $\mu\text{m}$ , and >150  $\mu\text{m}$ . The BR grain size distribution displays prominent modes for the fine and coarse fractions, while the medium fraction displays a bimodal spectrum likely due to smaller chlorite grains adhering to larger grains during sieving.

### 3.2. Mineralogical and chemical compositions of powdered basalts

Mineralogical and chemical compositions of BR and PV basaltic powders show differences that are likely to influence weathering rate and hence CDR potential by ERW (Table 3 through 5; Figs. 3 and 4). Notable mineralogical differences exist between the BR and PV powders regardless of size fraction, where the metamorphosed BV powder contains chlorite, epidote, plagioclase, actinolite, quartz and Fe/Ti oxides, compared to the unmetamorphosed PV which is dominated by plagioclase feldspar and pyroxene (mainly clinopyroxene) with small amounts of Fe/Ti oxides, quartz, and 2:1 phyllosilicates that appear to be a mix of chlorite and vermiculite (April and Keller, 1992) (Table 3, Fig. 3).

The chemical compositions of BR and PV (Table 4) are more similar than the mineralogical compositions of these two basaltic powders. BR is more Si-rich than PV, and PV contains higher amounts of Al, Mg and Ti than BR, but both BR and PV primarily plot in the basalt field on a TAS diagram (Fig. 4), where the one exception is the coarse fraction of PV, which plots on the boundary of basalt and basaltic andesite.

Differences in mineralogy as a function of grain size are observed among size fractions for both basaltic powders, especially in BR where

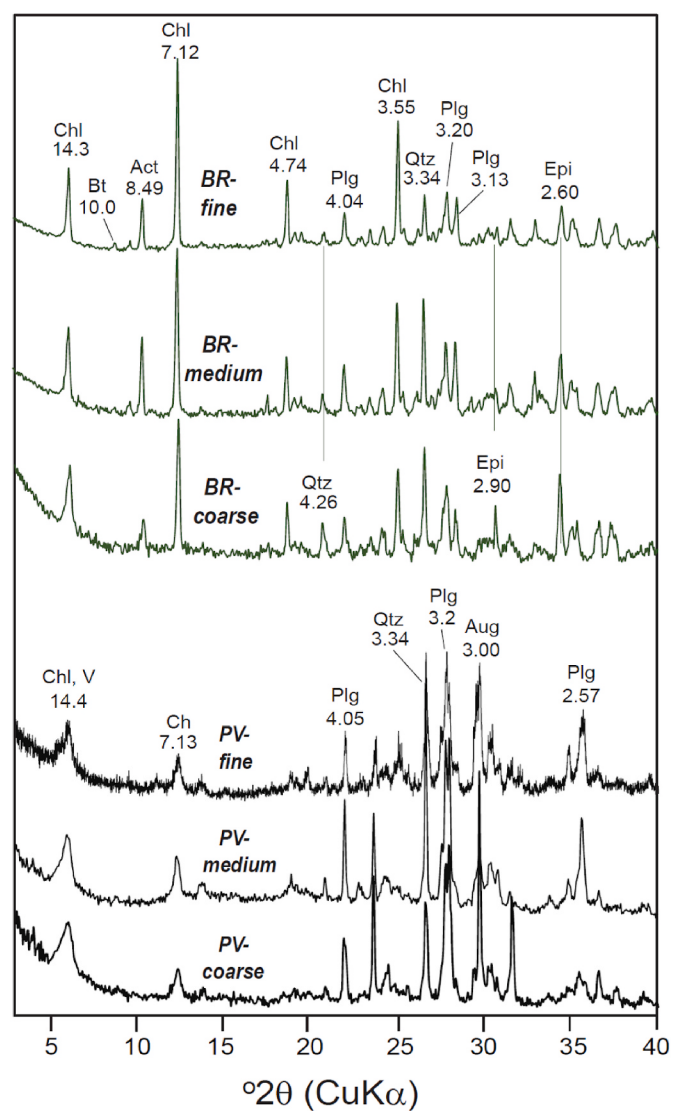


**Fig. 3.** XRD data for the three size fractions of the two samples provide evidence for mineralogical differences between the two samples (BR vs. PV) as well as among size fractions for a given sample. Diagnostic peaks are indicated with d-spacings in Å shown below mineral abbreviations. Chl = chlorite (clinochlore), V = vermiculite, Bt = biotite, Act = actinolite, Qtz = quartz, Plg = plagioclase feldspar, Epi = epidote.

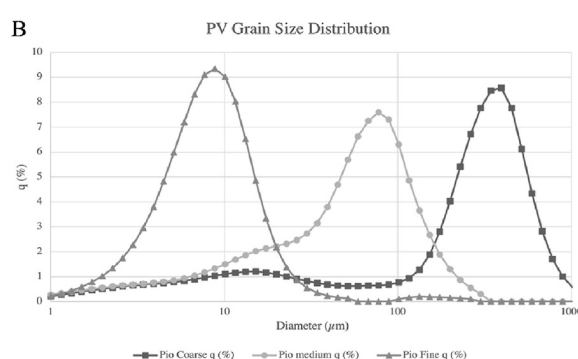
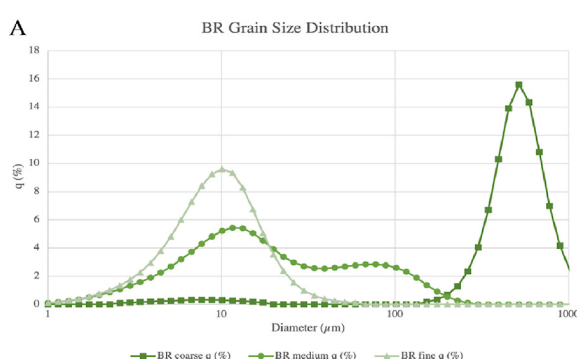


**Fig. 2.** Results of grain size separation by sieving for (A) BR and (B) PV powdered rocks. Note three prominent modes in the PV sample; also note prominent modal ranges for BV fine and coarse fractions, and bimodal spectrum for the medium-size sample of BR.

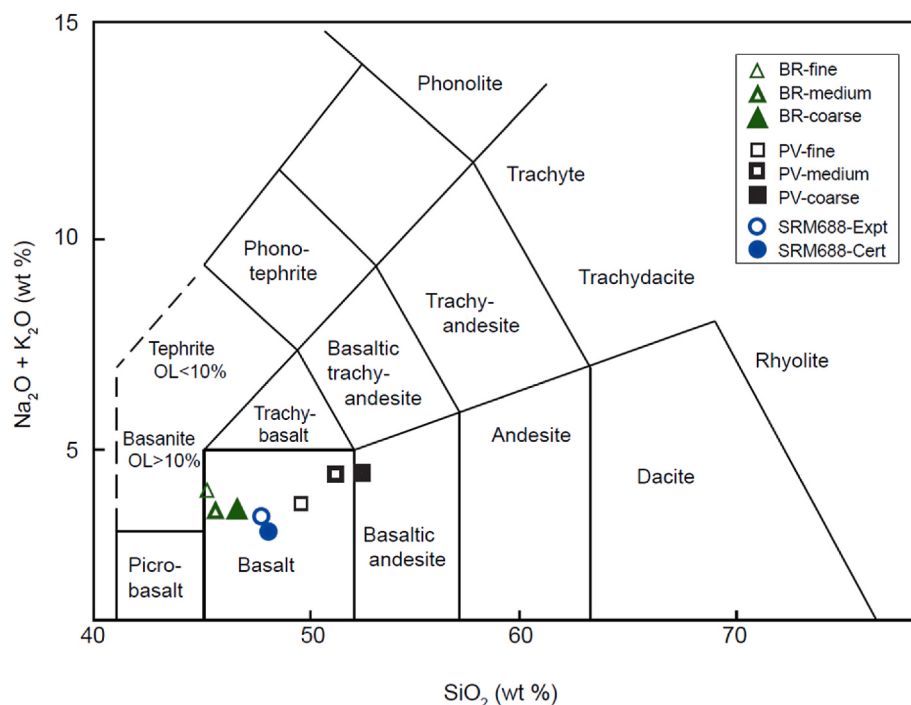


**Fig. 4.** Size fractions of powdered BR and PV rocks as well as SRM688 basalt certified value (Cert) and SRM688 analyzed in-line experimentally (Expt), all plotted as  $\text{SiO}_2$  vs. total alkalis (Le Maitre, 2002). All powders except the coarse fraction of PV plot in the basalt field; PV-coarse exhibits a borderline basalt to basaltic andesite composition.

the greatest difference in mineralogy is the high amount of chlorite in the fine fraction of BR compared to the medium and coarse fractions (Table 3). The abundance of chlorite in the BR fine fraction (51%) is 2.5 times greater than chlorite in the coarse fraction (19%), and the abundance of chlorite in the medium fraction of BR is intermediate to the fine and coarse fractions. Epidote and actinolite vary inversely with chlorite, increasing in abundance with increasing grain size. In the PV sample, pyroxene and plagioclase are inversely correlated – note that with decreasing grain size, pyroxene increases slightly as plagioclase

decreases. Overall, differences across grain size fractions are much more pronounced in BR due to the concentration of chlorite in the fine fraction.

### 3.3. Mineral compositions and textures in the basaltic powders: SEM/EDS

SEM imaging depicts distinct textural differences between BR and PV (Fig. 5). BR contains elongated actinolite and platy chlorite crystals mixed with blocky-to-equant crystals of plagioclase and epidote

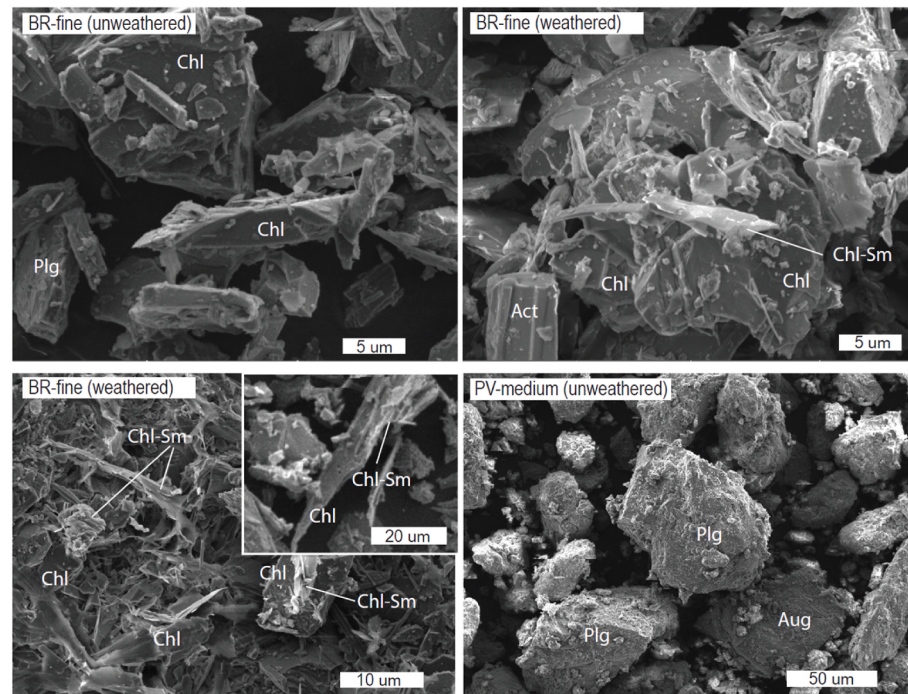


**Fig. 5.** SEM images showing unweathered BR-fine in upper left, and unweathered PV-medium at lower right. Note presence of platy chlorite (Chl) in BR as well as plagioclase (Plg) and actinolite (Act). PV is dominated by ~ equant Plg and augite (Aug). Examples of textural and compositional changes with weathering are shown in the upper right and lower left (both BR-fine), notably grains of chlorite with frayed and curled edges and compositions intermediate to chlorite and smectite (Chl-Sm).

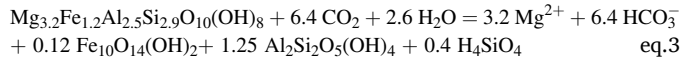
whereas PV is dominated by blocky-to-equant crystals of plagioclase and pyroxene. EDS analysis of clean mineral faces (proper orientation, absence of adhered grains) was used to produce the data on mineral compositions which are reported as mean values in [Table 5](#).

SEM imaging of powders exposed to experimental weathering showed distinct changes in texture, especially in the fine fraction of BR, where frayed and curled edges of chlorite grains produce compositions, e.g.  $\text{Ca}_{0.17}\text{Na}_{0.17}(\text{Al}_{0.27}\text{Fe}_{0.97}\text{Mg}_{2.03})(\text{Si}_{2.67}\text{Al}_{1.33})\text{O}_{10}(\text{OH})_2$ , which are intermediate to unweathered chlorite ([Table 5](#)) and pedogenic smectite ([Ryan and Huertas, 2009](#)), indicating leaching of Mg and sorption of Ca and Na ([Fig. 5](#)). Textural changes to PV are less evident, but numerous EDS spectra from weathered PV powders produced stoichiometries that indicate leaching of base cations, especially leached augite with low Mg and Ca and also plagioclase grains with Na and Ca content <50% of stoichiometric plagioclase.

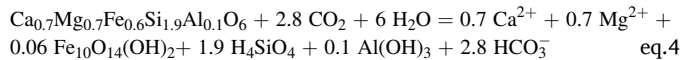
#### 3.4. Leachate results of the weathering experiment: ICP-MS

ICP-MS analysis of leachates provides data on base cations leached from primary minerals during experimental weathering, and as such can be used as a proxy for assessing weathering rates in the presence of  $\text{CO}_2$ . Carbon dioxide reduction (CDR) rates were calculated based on the weathering reactions in equations 3–5. Mineral compositions are based on SEM-EDS data. The main minerals showing evidence of weathering in Pioneer Valley basalt are augite and plagioclase, and in the case of Blue Ridge meta-basalt, the abundance of chlorite relative to amphibole in BR – combined with evidence of weathered chlorite in post-weathering SEM analyses – indicates that chlorite is the main factor controlling CDR potential in Blue Ridge meta-basalt. This inference is consistent with findings of [Buss et al. \(2008\)](#) who found that chlorite weathers more rapidly than hornblende in tropical soils of Luquillo Puerto Rico.

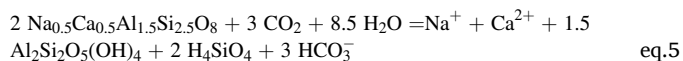
##### Chlorite



##### Augite



##### Na-Ca plagioclase



Conversion of  $\text{CO}_2$  to  $\text{HCO}_3^-$  balances the positive charge of soluble cations e.g.  $\text{Ca}^{2+}$  and  $\text{Mg}^{2+}$  that are released from silicate minerals during weathering. This study provides no direct measurement of dissolved bicarbonate in weathering experiment leachates, so CDR is based on stoichiometry of these reactions, and given that weathering of Ca and Mg silicate minerals are primarily responsible for CDR ([Beerling et al., 2020](#); [Lewis et al., 2021](#)), all CDR calculations are based on these two elements as shown in equations 3–5. In the case of augite for example (eq. 4), for 1.4 mol of divalent Ca + Mg (0.7 mol of each) present in leachate, 2.8 mol of  $\text{CO}_2$  would be consumed and converted to  $\text{HCO}_3^-$ . Using PV-Fine as an example, 1175 mg (48.32 mmol) of Mg were leached out of the basalt in the experimental soil profile per kg (of basaltic powder), and 357 mg (8.91 mmol) of Ca per kg of basaltic powder were leached. The sum total of 57.23 mmol (Mg + Ca) leached per kg of basaltic powder over the two-week weathering experiment corresponds to conversion of 114.5 mmol of  $\text{CO}_2$  to  $\text{HCO}_3^-$  based on the stoichiometry in eq. 4. When scaled up to an application rate of 50 tons of powdered basalt (1 mm thick) per ha, and when the time frame is extrapolated from two weeks to one year, the carbon dioxide reduction (CDR) potential for PV-Fine is 6.55 tonnes of  $\text{CO}_2/\text{ha}/\text{yr}$  ([Fig. 8](#)) for a tropical environment receiving 2000–2500 mm of mean annual precipitation.

As shown in [Figs. 6–8](#), BR and PV exhibit relatively similar weathering fluxes based on cumulative Ca and Mg present in leachates analyzed by ICP-MS. Mg and Fe were the elements present at the highest concentrations in BR leachates with Mg approximately double the amount of Fe ([Fig. 6](#)); Mg and Fe were also the most abundant elements in PV leachates in approximately equal molar concentrations. Fe was not used in CDR calculations because of the possibility that much of it is derived from hydrolysis of Fe oxides or hydroxides. In powders of both BR and PV, Na, K, Ca, and Mn are also present in leachates, but at order-of-magnitude lower concentrations than Mg (and Fe), and as expected, the fine fractions of both basaltic powders (BR and PV) display the greatest extent of cation leaching, indicating that the fine fractions experience the fastest weathering fluxes relative to medium and coarse fractions of the same powders. Relatively low amounts of Na and Ca in leachate compared to Mg and Fe indicate that plagioclase weathering occurred slowly relative to chlorite in BR, and to augite in PV. Relatively low amounts of Si compared to other cations in leachate are likely due to saturation that can cause formation of solid phases and lead to lower-than-expected concentrations in solution ([Yokoyama and Banfield, 2002](#)).

The extent of weathering can be assessed by comparing the amount of a given cation leached into solution ([White et al., 1998](#)) relative to the amount of that cation in the original pre-weathering powder ([Table 4](#)). Doing so indicates that 1.20–1.82% of total Mg in the rock powder was leached from BR and that the % Mg leached was highest in the fine fraction. This is true for all elements with few exceptions, further emphasizing the greater reactivity of the fine fraction. In the case of BR, the abundance of weatherable chlorite in the fine fraction adds a mineralogical variable to the influence of grain size on weathering rate, whereas for the PV powders, mineralogy varies minimally with grain size and thus increased weathering in the fine fraction is driven almost solely by grain size (see [Table 6](#)).

Examining the results of leaching over the 14-day duration of the experiment shows how solution compositions evolved over time ([Fig. 7](#)). For both BR and PV, the fine fractions weather the fastest, and cumulative leaching of Ca and Mg plots along linear to slightly parabolic curves over time, typical arcs for weathering reactions over time in the tropics ([Fisher and Ryan, 2006](#)). As shown in [Fig. 7](#), BR-coarse leachates contained the lowest amount of calcium throughout the experiment (totaling 2.07 mmol/kg Ca at the end of the sixth round, hour 336) compared to the BR-medium fraction (leachates total 2.78 mmol/kg Ca), and BR-fine displays the highest amount of Ca leaching totaling 3.98 mmol/kg Ca (0.36% of Ca in the basaltic powder fine fraction). Likewise, leaching of Ca from PV displays a similar trend, where the coarse size fraction totaled 3.98 mmol/kg Ca leached at the end of the experiment, compared to 6.40 mmol/kg Ca leached from PV-medium and 8.81 mmol/kg Ca leached from PV-fine (0.47% of Ca in the basaltic powder fine fraction). A similar comparison can be made for Mg, where the fine fractions produced leachates with 1.5–2 times as much Mg as the coarse fractions of BR and PV.

Quantifying the two divalent cations ( $\text{Ca}^{2+}$  and  $\text{Mg}^{2+}$ ) present in solutions leached from basaltic powders produced the overall carbon dioxide reduction (CDR) potential ([Fig. 8](#)). BR displays lower CDR potential for the coarse and medium size fractions in comparison to PV; however, the fine fractions of BR and PV display nearly the same CDR (6.5 vs. 6.8 t/ha/y). Furthermore, the fine fractions have greater CDR potentials in comparison to the coarse and medium size fractions. The regression curves fit to the data points produce high  $R^2$  values (0.998 and 0.948) but relatively low p-values (0.29 and 0.44 at 95% confidence) that reflect the low number of data points. Overall, increasing CDR with decreasing grain size for both BR and PV is consistent with expectations, and the similarities in rate (cation flux) vs. grain size between BR and PV are notable.

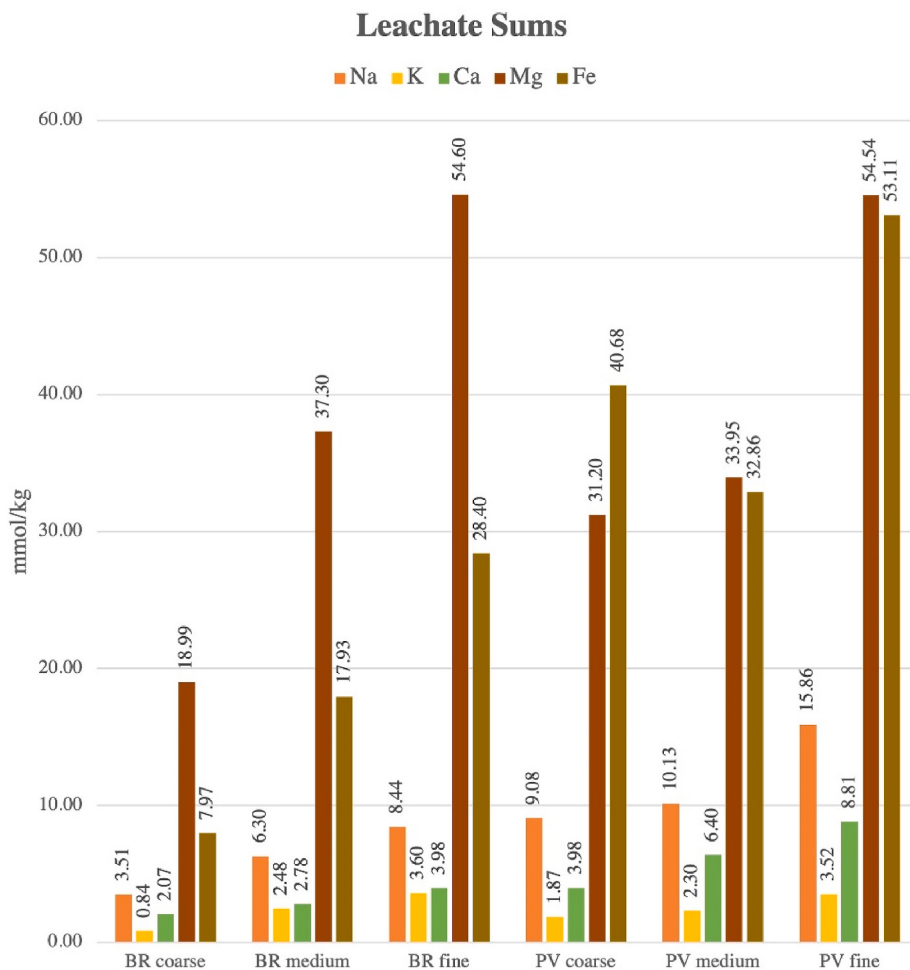


**Fig. 6.** Leachate sums of Na, K, Ca, Mg, Fe and Mn (mmol leached per kg of rock powder) as a function of grain size for the two powdered basaltic rocks BR and PV.

#### 4. Discussion

The goals of this study were to (1) experimentally determine weathering potential of two different basalts as a function of grain size, and (2) assess implications for carbon dioxide reduction (CDR) by means of enhanced rock weathering (ERW), an approach that consists of applying basaltic powders of varied grain size to fields or forests. It is well known that finer grain size and higher reactive surface area enhance rate of chemical weathering (e.g. Brantley, 2008), yet relatively little empirical information is available to assess the significance of grain size as it may affect CDR (Renforth et al., 2015). Results of this study indicate a two-fold increase in leaching of cations (Fig. 8) over a ~ order of magnitude grain size decrease, where the rate doubles from fine-medium sand (~250–500  $\mu\text{m}$  mode) to a fraction dominated by silt + clay (~10  $\mu\text{m}$  mode) (Fig. 2; Table 2). Also notable is that as grain size decreases below 100  $\mu\text{m}$ , the weathering flux appears to increase exponentially (Fig. 8). Theoretical models and calculations considering ERW potential of powdered basalts show similar exponential curves with decreasing grain size (Rinder and von Hage, 2021).

CDR and weathering flux calculations presented herein are based on the fact that  $\text{CO}_2$  that is dissolved in weathering solutions (e.g. soil water) is a reactant that is transformed into dissolved bicarbonate, with examples pertaining to BR and PV shown as chemical reactions in equations 3–5. Mg and Ca are stoichiometrically linked to  $\text{CO}_2$  in silicate weathering reactions and are used in this study to determine CDR. K, Na, Al, Fe and Si are not considered in these calculations given that Mg and Ca are the main elements responsible for CDR by ERW (Beerling et al.,

2020). Fe and Mn are not included because they may be derived from iron oxides, although Fe could be a divalent cation released along with Mg e.g. by weathering of chlorite. Si and Al, while certain to be liberated from mineral structures by weathering of silicates, are not a factor in stoichiometric calculations of CDR based on equations 1–5.

The differing mineralogical and chemical compositions between basalts and within the different grain sizes of each basalt influence weathering flux. The two minerals that weathered the fastest appear to be chlorite (in BR) and augite (in PV). The abundance of chlorite in BR suggests that it likely will be the phase that drives weathering in metamorphosed basalts like BR (Price et al., 2012) whereas pyroxene is likely to drive early stages of weathering of unmetamorphosed basalts like PV (Behrens et al., 2015; Pincus et al., 2017). The increased rate (cation flux) with decreasing size fraction for both BR and PV is attributed to increased reactive surface area; in the case of BR, the high % of chlorite in the fine fraction (51%) means an abundance of Mg-O bonds in octahedral sites chlorite, which are prone to hydrolysis in acidic soils like those of tropical ecosystems (Wilson, 2004).

Relatively low amounts of Na and Ca in leachates is attributed to slower weathering of plagioclase relative to Mg-rich chlorite (in BR) and augite (in PV) (Rowe and Brantley, 1993; Pincus et al., 2017) – these Mg minerals are driving weathering. Preferential dissolution of Mg-rich chlorite is driven by the relatively weak Mg-O bond (362 kJ/mol) in the octahedral sheet of chlorite (Kohut and Warren, 2002; Ryan et al., 2008) and this factors into the high amount of Mg leached from BR; in pyroxenes, the relatively weak Mg-O bond (394 kJ/mol) compared to Ca-O bond (464 kJ/mol) (Nesbitt et al., 2017), combined with

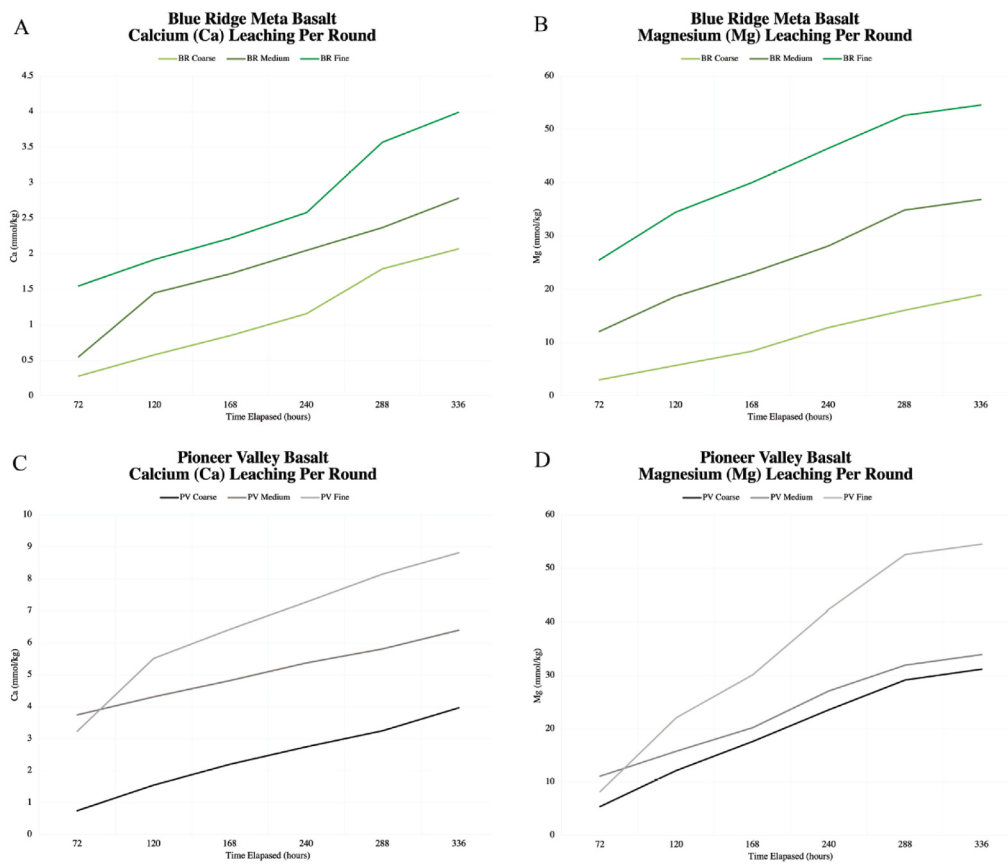


**Fig. 7.** Ca and Mg in leachates showing cumulative weathering losses from basaltic powders over time in elapsed hours, plotted as mg of element per kg of initial powder. Note higher rates with decreasing grain size e.g. more than twice as much Mg was leached out of BR Fine (54.6 mmol) compared to BR Coarse (19.0 mmol). BR Ca (A), BR Mg (B), PV Ca (C), PV Mg (D).

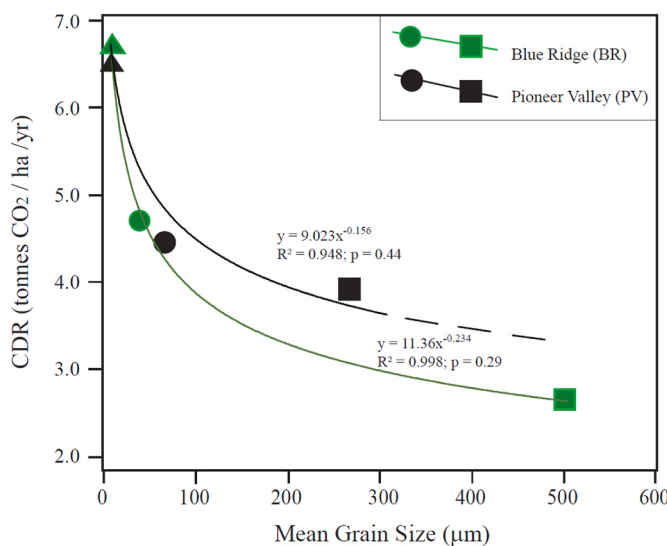


**Fig. 8.** Differences in potential for carbon dioxide reduction (CDR, C sequestration) as a function of mean grain size for the basaltic powders analyzed in this study. The CDR potential here is determined for a scenario where 50 tons of basaltic powder are applied per hectare in the humid tropics.

chronosequence-based evidence indicating that plagioclase outlasts augite during weathering of tropical soils, likely explains high amounts of Mg compared to Ca in PV leachates.

Incomplete leaching of Mg and Ca from the matrix of the weathering basalt powders is indicated by SEM analysis, mainly as Mg retention in 2:1 clays formed by weathering of chlorite, and Ca retention by adsorption to clays and incorporation into sparse micron-size rhombohedral calcite crystals. Thus, solutions in contact with solid phases (e.g. smectite, calcite) that might incorporate Mg or Ca appear to be at least locally saturated, a phenomenon that would limit leaching of the elements, meaning that Mg and Ca in leachates could lead to an underestimate of CDR. Regarding Mg, when plotted on a soil mineral stability diagram (Fig. 9), leachate concentrations of Mg<sup>2+</sup>, H<sup>+</sup> and H<sub>4</sub>SiO<sub>4</sub> coincide with the stability field of kaolinite and slightly overlap with Mg-smectite, implying that for the most-buffered, most-Mg rich solutions, Mg-smectite is at least locally stable. This is consistent with SEM observations of frayed edges of chlorite altered to Mg-smectite. Regarding Ca, using a K<sub>CO<sub>2</sub></sub> of 10<sup>-1.57</sup> for 35 °C (Plummer and Busenberg, 1982) and a range of dissolved CO<sub>2</sub> from 0.01 atm (typical of soils) to 0.0004 atm (air), dissolved Ca in solution in equilibrium with calcite would range from 52.0 mg/L (at 0.01 atm) to 19.2 mg/L (in equilibrium with air), the latter of which is similar to the highest Ca concentrations observed in leachates (19.4 mg/L in PV-fine and 22.5 mg/L in PV-medium; Table S1); in the majority of leachates, however, Ca appears to be below saturation. Thus, while precipitation of Mg or Ca in clays or carbonates would lead to underestimates of CDR by our approach, it is important to note that reprecipitation (e.g. into Mg-smectite or calcite) does not affect net CDR given that the Mg or Ca has been released from a primary silicate mineral by a reaction that consumes CO<sub>2</sub>; however, when quantification is based on leachate concentrations, as it is here, reprecipitation would cause CDR potential to be underestimated.

Experimental weathering resulted in similar (2.8–6.8 t CO<sub>2</sub>/ha/yr) flux-based rates for BR and PV, where the greatest differences were

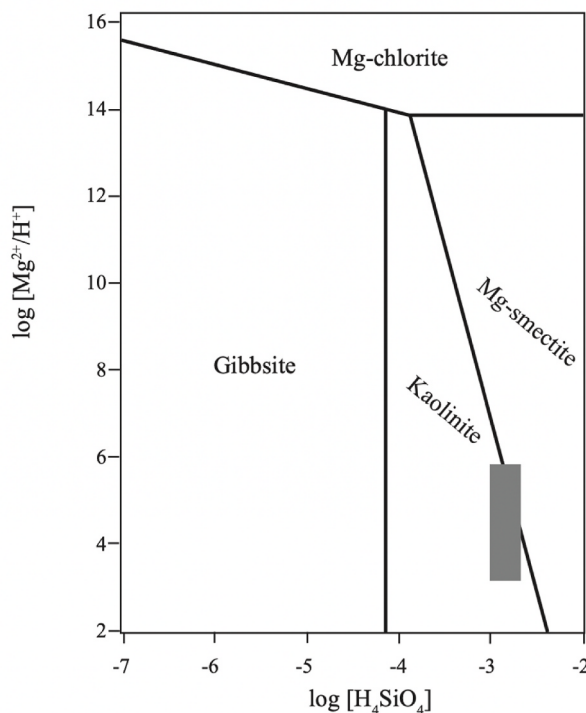


**Fig. 9.** Mineral stability diagram for an Mg-rich soil system consisting of Mg-Al-Si-O-H (modified from Lee et al., 2003). The weathering of basalts produces leachates that are mainly in the kaolinite stability field; however, leachates from the finest grain sizes (e.g. PV-fine, BR-fine) plot in the upper right of the range and slightly overlap with the stability field of Mg-smectite.

among grain size fractions within a given basaltic powder. Comparing this study's empirical results to modeled weathering rates shows some range in CDR potential. With geochemical reactive transport modeling, Kelland et al. (2020) estimated CDR potential between 2 and 4 t CO<sub>2</sub>/ha within one to five years after a single application of basaltic rock dust in a northern European climate. Kantzias et al. (2022) used dynamic carbon budget modeling to assess the CO<sub>2</sub> removal potential and agricultural benefits of implementing ERW across arable croplands in the United Kingdom, finding that enhanced rock weathering could deliver net carbon dioxide removal of 6–30 MtCO<sub>2</sub> yr<sup>-1</sup> for the UK by 2050. This would represent up to 45% of CDR required nationally to meet net-zero emissions. Assuming that this applies to the 3.7 million hectares of arable cropland as reported by the UK department for Environment, Food, and Rural Affairs (available at [www.gov.uk/government/statistics/](http://www.gov.uk/government/statistics/)), sequestration rate (CDR) would be 1.6–8.1 t CO<sub>2</sub>/ha/yr. Lastly, using reactive transport modeling simulations based on measured mineral composition and N<sub>2</sub>-gas BET specific surface area (SSA), Lewis et al. (2021) estimate CDR between 1.3 and 8.5 t CO<sub>2</sub> ha<sup>-1</sup> within 15 years following a baseline application of 50 t ha<sup>-1</sup> basalt for a climate simulating northern Europe. Notably, Lewis et al. (2021) found that CDR rates double with a 10-fold increase in reactive surface area, similar to the doubling of reaction rate in our experiment with a ~10-fold decrease in modal grain size. Given that this is an experimental study, factors related to soil permeability and leaching potential will factor into how such results might actually manifest themselves in the natural environment.

The two-fold increase in weathering flux across a grain size difference of fine silt vs. fine-medium sand provides important considerations for rate of CDR by ERW. In addition to the effect of grain size of basaltic powders demonstrated herein, additional factors influencing CDR rates include climate, time, mineral/chemical compositions, and discrepancies between modeling and field applications (e.g. Edwards et al.,

2017; Paulo et al., 2021; Beerling et al., 2020; Lewis et al., 2021). Given the complexity of weathering environments in agricultural ecosystems, we recognize that there is a need for field trials involving agricultural lands in the tropics. Experimental approaches always have some limitations when scaled to the natural world; for example, these experiments were carried out at constant temperature, so diurnal changes in temperature are not considered, nor are potential influences of microbial communities or mixing downward into the soil profile. We also extrapolate a 2-week experiment out to annual CDR, so the data here may include early-stage weathering of the most susceptible minerals that could cause an overestimate of the longer-term rate; therefore, longer trials, ideally in the field, will be important. In addition to the importance of grain size and mineralogy, other considerations involving implementation of ERW at large include climate, suitable agricultural lands, availability of basaltic rocks, and CO<sub>2</sub> emissions from mining, comminution, and transport. In spite of these limitations, it is worth noting that the CDRs determined from this experimental approach are comparable to (and in some cases higher than) rates determined in other experimental and modeling studies (e.g. ten Berge et al., 2012; Renforth et al., 2015; Dietzen et al., 2018; Amann et al., 2020; Kelland, 2020; Lewis et al., 2021).

In addition to data on weathering rates of varied basaltic rocks under a range of soil-climate conditions, future studies like that of Beerling et al. (2020) should consider socio-economic factors or life cycle assessment centered around the sustainability of mining, transport, and crushing the rock up to fine grain sizes, thus allowing for a net CO<sub>2</sub> sequestration with all costs involved in the process. Likewise, studies should also assess how often applications of basaltic powder to field sites should take place. There is a long history of beneficial anthropogenic alterations of soil in the tropics, notably practices used to create terra preta soils as ancient as 2500 years old in the Amazon basin, where informed environmental management created sustainably fertile soils from native acidic nutrient-poor Oxisols that retain their soil quality to the present day (Lima et al., 2002).

## 5. Conclusions

Mg-rich silicates (chlorite, augite) were the main minerals affected by the experimental weathering design employed in this study, an observation that is consistent with field-based observations of mafic rocks in weathering environments. Weathering fluxes for chlorite and augite approximately double from sand-sized (~250–500 μm) to silt-sized (<45 μm), and this has implications for forecasting potential for carbon dioxide reduction (CDR) by means of enhanced rock weathering (ERW) of basaltic powders applied to fields as a negative emission technology (NET). In particular, CDR rates vary by a factor of two, ranging from fine-medium sand of BR and PV basaltic powders (3–4 t/ha/yr), compared to a rate of 6–7 t/ha/yr for fine-medium silt.

## Availability of data and material

In addition to tables and figures presented in this ms, results of raw rock powder XRF analyses and leached solution ICP-MS analyses are available at <https://middlebury.figshare.com/>, with unique DOI link as follows: <https://doi.org/10.57968/Middlebury.22933439>. Residual rock fragments and powders are stored in Bicentennial Hall at Middlebury College and are available by request: [pryan@middlebury.edu](mailto:pryan@middlebury.edu).

## Declaration of competing interest

The authors declare the following financial interests/personal relationships which may be considered as potential competing interests: Peter Ryan reports financial support was provided by Middlebury College.

## Data availability

Data will be made available on institution website as indicated in the ms

## Acknowledgments

Powdered basaltic samples (Blue Ridge and Pioneer Valley) were provided by Rock Dust Local LLC of Bridport, Vermont USA. Conversations with Amy Lewis, Binoy Sarkar and Peter Wade were helpful in study design. Allison Jacobel assisted with data analysis, Jody Smith assisted with SEM, and anonymous reviewers and the editorial team are thanked for the way they improved the original manuscript. Financial support was provided by the Malcolm McCallum Fund in the Middlebury College Department of Earth and Climate Sciences.

## Appendix A. Supplementary data

Supplementary data to this article can be found online at <https://doi.org/10.1016/j.apgeochem.2023.105728>.

## References

- Amann, T., Hartmann, J., Struyf, E., de Oliveira Garcia, W., Fischer, E.K., Janssens, I., et al., 2020. Enhanced Weathering and related element fluxes – a cropland mesocosm approach. *Biogeosciences* 17, 103–119. <https://doi.org/10.5194/bg-17-103-2020>.
- Anbeek, Chris, 1993. The effect of natural weathering on dissolution rates. *Geochem. Cosmochim. Acta* 57 (Issues 21–22), 4963–4975. [https://doi.org/10.1016/S0016-7037\(05\)80002-X](https://doi.org/10.1016/S0016-7037(05)80002-X). ISSN 0016-7037.
- April, R.H., Keller, D.M., 1992. Saponite and vermiculite in amygdales of the Granby basaltic tuff, Connecticut Valley. *Clay Clay Miner.* 40, 22–31.
- Banfield, J.F., Nealson, K.H., 1997. Geomicrobiology: Interactions between Microbes and Minerals. *Mineralogical Society of America*.
- Beerling, D.J., Kantzas, E.P., Lomas, M.R., Wade, P., Eufrasio, R.M., Renforth, P., et al., 2020. Potential for large-scale CO<sub>2</sub> removal via enhanced rock weathering with croplands. *Nature* 583, 242–248. <https://doi.org/10.1038/s41586-020-2448-9>.
- Behrns, R., Bouchez, J., Schuessler, J.A., Dultz, S., Hewawasam, T., von Blanckenburg, F., 2015. Mineralogical transformations set slow weathering rates in low-porosity metamorphic bedrock on mountain slopes in a tropical climate. *Chem. Geol.* 411, 283–298. <https://doi.org/10.1016/j.chemgeo.2015.07.008>.
- Brantley, S.L., 2008. Kinetics of mineral dissolution. In: Brantley, S.L., Kubicki, J.D., White, A.F. (Eds.), *Kinetics of Water-Rock Interaction*. Springer, New York, pp. 151–196.
- Bray, Andrew W. Oelkers, Bonneville, Eric H., Wolff-Boenisch, Steeve, Potts, Domenik, Fones, Nicola J., Gary, Benning, Liane, G., 2015. The effect of pH, grain size, and organic ligands on biotite weathering rates. *Geochem. Cosmochim. Acta* 164, 127–145. <https://doi.org/10.1016/j.gca.2015.04.048>.
- Buss, H.L., Sak, P.B., Webb, S.M., Brantley, S.L., 2008. Weathering of the rio blanco quartz diorite, Luquillo mountains, Puerto Rico: coupling oxidation, dissolution, and fracturing. *Geochem. Cosmochim. Acta* 72, 4488–4507.
- Calabrese, S., Wild, B., Bertagni, M.B., Bourg, I.C., White, C., Aburto, F., Cipolla, G., Noto, L.V., Porporato, A., 2022. Nano to global-scale uncertainties in terrestrial enhanced weathering. *Environ. Sci. Technol.* 56, 15261–15272. <https://doi.org/10.1021/acs.est.2c0316>.
- Dietzen, C., Harrison, R., Michelsen-Correa, S., 2018. Effectiveness of enhanced mineral weathering as a carbon sequestration tool and alternative to agricultural lime: an incubation experiment. *Int. J. Greenh. Gas Control* 74, 251–258. <https://doi.org/10.1016/j.ijggc.2018.05.007>.
- Edwards, D.P., Lim, F., James, R.H., Pearce, C.R., Scholes, J., Freckleton, R.P., Beerling, D.J., 2017. Climate change mitigation: potential benefits and pitfalls of enhanced rock weathering in tropical agriculture. *Biol. Lett.* 13, 20160715 <https://doi.org/10.1098/rsbl.2016.0715>.
- Fisher, G.B., Ryan, P.C., 2006. The smectite to disordered kaolinite transition in a tropical soil chronosequence, Pacific Coast, Costa Rica. *Clay Clay Miner.* 54, 571–586.
- Holdren, G.R., Speyer, P.M., 1987. Reaction rate-surface area relationships during the early stages of weathering. II. Data on eight additional feldspars. *Geochem. Cosmochim. Acta* 51, 2311–2318.
- Kantzas, E.P., Val Martin, M., Lomas, M.R., et al., 2022. Substantial carbon drawdown potential from enhanced rock weathering in the United Kingdom. *Nat. Geosci.* 15, 382–389. <https://doi.org/10.1038/s41561-022-00925-2>.
- Kelland, et al., 2020. Increased yield and CO<sub>2</sub> sequestration potential with the C4 cereal Sorghum bicolor cultivated in basaltic rock dust-amended agricultural soil. *Global Change Biol.* 26, 3658–3676.
- Lal, R., 1995. *Sustainable Management of Soil Resources in the Humid Tropics*, 876. United Nations University Press.
- Le Maître, R.W., 2002. Igneous Rocks a Classification and Glossary of Terms Recommendations of the International Union of Geological Sciences, Sub-commission on the Systematics of Igneous Rocks. Cambridge University Press, p. 236. <https://doi.org/10.1017/CBO9780511535581>.
- Lee, B.D., Sears, S.K., Graham, R.C., Amrhein, C., Vali, H., 2003. Secondary mineral genesis from chlorite and serpentine in an ultramafic soil toposequence. *Soil Sci. Soc. Am. J.* 67, 1309–1317. <https://doi.org/10.2136/sssaj2003.1309>.
- Lewis, A.L., Sarkar, B., Wade, P., Kemp, S.J., Hodson, M.E., Taylor, L.L., et al., 2021. Effects of mineralogy, chemistry and physical properties of basalts on carbon capture potential and plant-nutrient element release via enhanced weathering. *Appl. Geochem.* 132, 105023 <https://doi.org/10.1016/j.apgeochem.2021.105023>.
- Nesbitt, H.W., Cormack, A.N., Henderson, G.S., 2017. Defect contributions to the heat capacities and stabilities of some chain, ring, and sheet silicates, with implications for mantle minerals. *Am. Mineral.* 102, 2220–2229. <https://doi.org/10.2138/am-2017-6103>.
- Paulo, C., Power, I.M., Stubbs, A.R., Wang, B., Zeyen, N., Wilson, S.A., 2021. Evaluating feedstocks for carbon dioxide removal by enhanced rock weathering and CO<sub>2</sub> mineralization. *Appl. Geochem.* 129, 104955 <https://doi.org/10.1016/j.apgeochem.2021.104955>.
- Pincus, L.N., Ryan, P.C., Huertas, F.J., Alvarado, G.E., 2017. The influence of soil age and regional climate on clay mineralogy and cation exchange capacity of moist tropical soils: a case study from Late Quaternary chronosequences in Costa Rica. *Geoderma* 308, 130–148. <https://doi.org/10.1016/j.geoderma.2017.08.033>.
- Plummer, L.N., Busenberg, E., 1982. The solubilities of calcite, aragonite and vaterite in CO<sub>2</sub>-H<sub>2</sub>O solutions between 0 and 90°C, and an evaluation of the aqueous model for the system CaCO<sub>3</sub>-CO<sub>2</sub>-H<sub>2</sub>O. *Geochem. Cosmochim. Acta* 46, 1011–1040.
- Price, J.R., Rice, K.C., Szymanski, D.W., 2012. Mass-balance modeling of mineral weathering rates and CO<sub>2</sub> consumption in the forested, metabasaltic Hauer Branch watershed. Catoctin Mountain, Maryland, USA. *Earth Surface Processes and Landforms* 38, 859–875. <https://doi.org/10.1002/esp.3373>.
- Renforth, P., Pogge von Strandmann, P.A.E., Henderson, G.M., 2015. The dissolution of olivine added to soil: implications for enhanced weathering. *Appl. Geochem.* 61, 109–118. <https://doi.org/10.1016/j.apgeochem.2015.05.016>.
- Rinder, von Hagke, 2021. The influence of particle size on the potential of enhanced basalt weathering for carbon dioxide removal - insights from a regional assessment. *J. Clean. Prod.* 315, 128178 <https://doi.org/10.1016/j.jclepro.2021.128178>.
- Rohli, R.V., Vega, A.J., 2015. *Climatology*, third ed. Jones and Bartlett, p. 443.
- Rozalén, M., Ramos, M.E., Fiore, S., Gervilla, F., Huertas, F.J., 2014. Effect of oxalate and pH on chrysotile dissolution at 25 °C: an experimental study. *Am. Mineral.* 99, 589–600.
- Ryan, P.C., Huertas, F.J., 2009. The temporal evolution of pedogenic Fe-smectite to Fe-kaolin via interstratified kaolin-smectite in a moist tropical soil chronosequence. *Geoderma* 151, 1–15.
- Ryan, P.C., Hillier, S., Wall, A.J., 2008. Stepwise effects of the BCR sequential chemical extraction procedure on dissolution and metal release from common ferromagnesian clay minerals: a combined solution chemistry and X-ray powder diffraction study. *Sci. Total Environ.* 407, 603–614.
- Rowe, G.L., Brantley, S.L., 1993. Estimation of the dissolution rates of andesitic glass, plagioclase and pyroxene in a flank aquifer of Poás Volcano, Costa Rica. *Chem. Geol.* 105, 71–87.
- ten Berge, H.F.M., van der Meer, H.G., Steenhuijen, J.W., Goedhart, P.W., Knops, P., et al., 2012. Olivine weathering in soil, and its effects on growth and nutrient uptake in ryegrass (*Lolium perenne* L.): a pot experiment. *PLoS One* 7 (8), e42098. <https://doi.org/10.1371/journal.pone.0042098>.
- White, A.F., Blum, A.E., Schulz, M.S., Vivit, D.V., Stonestrom, D.A., Larsen, M.C., Murphy, S.F., Eberl, D., 1998. Chemical weathering in a tropical watershed, Luquillo Mountains, Puerto Rico: I. Long-term versus short-term weathering fluxes. *Geochem. Cosmochim. Acta* 62, 209–226.
- White, A.F., Blum, A.E., Bullen, T.D., Vivit, D.V., Schulz, M., Fitzpaterich, J., 1999. The effect of temperature on experimental and natural chemical weathering rates of granitoid rocks. *Geochem. Cosmochim. Acta* 63, 3277–3291.
- Wilson, M.J., 2004. Weathering of the primary rock-forming minerals: processes, products and rates. *Clay Miner.* 39, 233–266.